Estimating Recent Global Sea Level Changes

H.-P. Plag
Nevada Bureau of Mines and Geology and Seismological Laboratory, University of Nevada, Reno, Mailstop 178, Reno, NV 89557, USA, e-mail: hpplag@unr.edu.

Abstract

An empirical model for sea level trends over several decades is set up such that it is consistent with the global pattern of Local Sea Level (LSL) trends observed by the global network of tide gauges. The forcing factors taken into account are steric sea level variations, present-day ice load changes, and post-glacial rebound. Model parameters are determined in a least squares fit of the model to the LSL trends. The model allows the determination of the contribution of each factor to the global average LSL trend.

Here we compare the solutions for two different LSL trend sets, namely one determined without and one with taking into account local atmospheric forcing at the tide gauges (denoted here as T1 and T2). From the globally given model, the global average trend over the last 50 years in LSL is found to be of the order of 1.05 ± 0.75 mm/yr and 1.20 ± 0.70 mm/yr for T1 and T2, respectively. For T1, the contribution of the Antarctic and Greenland ice sheets to the global average are 0.39 ± 0.11 mm/yr and 0.10 ± 0.05 mm/yr, respectively and for T2 0.31 ± 0.16 mm/yr and 0.16 ± 0.03 mm/yr, respectively. Using T1, the contribution from steric change is clearly identified and found to be at least 0.2 mm/yr with the most likely value being close to 0.35 mm/yr. For T2, there is no correlation between the spatial pattern of the observed LSL trends and the steric sea level trends, and the steric contribution to the global average turns out to be equal to zero. This result indicates a very high correlation between the local atmospheric forcing and the thermosteric sea level changes, which may be the result of a feedback of temperature changes in the upper layer of the ocean into the air pressure and wind field over the ocean.

Keywords: *global sea level rise, local sea level trends, ice sheets changes*

1 Introduction

The mass balance of the global water cycle is of paramount interest for understanding, predicting and mitigating the impact of climate change. Understanding the sea level changes over the last decades and century is a prerequisite for quantifying climate-related changes in the oceans volume and mass, as well as for establishing future sea level scenarios. Church et al. (2001) emphasize the considerable uncertainties in the mass balance of the ocean and, in consequence, the global sea level. In particular, the contribution of the large ice sheets to current sea level changes is rather uncertain.

The global mass and volume of the ocean are two absolute quantities characterizing the ocean as a reservoir in the global hydrological cycle. Changes in these quantities are directly related to changes in the hydrological cycle and therefore to climate change. Local Sea Level (LSL), which is defined here as the (absolute) vertical distance between the surface of the ocean and the surface of the solid Earth, depends on the distribution of the ocean water in a given topography of the Earth surface. Thus, LSL depends on many different factors, such as the Earth's topography, the (time-variable) geoid, changes of the Earth's rotation, atmospheric circulation, heat and salinity distribution in the ocean, ocean circulation, past and present mass movements in the Earth system, the visco-elastic properties of the Earth's interior, sedimentation, and even anthropogenic subsidence due to groundwater, gas, and oil extraction. At coastal locations, LSL is measured relative to a benchmark on land, which, if properly chosen, follows the vertical motion of the land around the tide gauge, including the ocean bottom below it.

Over the last thirty years a number of studies have utilized the unique sea level data set provided by the *Permanent Service for Mean Sea Level* (PSMSL) for the determination of a global sea level rise (see Church et al., 2001, for a review). The global trends estimated in these studies range from +1 to +2.5 mm/yr. This relatively wide range mainly is due to the selection criteria used by the different researchers to select subsets of tide gauges as well as the methodology to determine a global trend. However, the link between LSL changes and changes in the global ocean mass and volume is complex and all forcing factors result in spatially highly variable trends. Taking into account that the global network of tide gauges only samples a small fraction of the ocean's surface, any estimate of a global rise not taking into account the spatial variability of the different contribution is bound to be biased.

In order to account for the spatial variability of the forcing, Plag (2006) derived a LSL balance equation that accounts for each forcing factor individually.

Using an approximate LSL equation which accounts for the contribution due to ocean temperature changes, post-glacial rebound, and the present-day changes in Greenland and Antarctica, he determined a global average rise in LSL of 1.05 ± 0.75 mm/yr. Here we extend this approach and study how the local atmospheric forcing affects the estimates of the global average.

In the next section, we briefly introduce the LSL equation and discuss the spatial fingerprint of the main forcing factors. In Section 3 we summarize the database used by Plag (2006), which is here complemented with an atmospheric dataset. Then, in Section 4 we consider the effect of the local forcing on the global grid of observed LSL trends. In Section 5, we introduce the regression model and in Section 6 discuss the effect of the local atmospheric forcing on the global estimates by comparing the results of Plag (2006), which do not account for the local atmospheric forcing, to the results obtained here after the local atmospheric forcing has been removed.

2 Local Sea Level Balance

For the discussion of secular trends, we approximate the monthly mean LSL $h_M(\vec{x},t)$ at a tide gauge located at a point $\vec{x}$ on the Earth surface as a sum of several factors, namely

$$\begin{aligned} h(\vec{x},t) \;=\; & S(\vec{x},t) + C(\vec{x},t) + A(\vec{x},t) + \\ & I(\vec{x},t) + G(\vec{x},t) + T(\vec{x},t) + \\ & P(\vec{x})(t-t_0) + V_0(\vec{x})(t-t_0) + \delta V(\vec{x},t) \end{aligned} \tag{1}$$

where t is time, t_0 an arbitrary time origin, and where we have considered the following contributions to LSL changes: S: steric changes, C: changes in ocean currents, A: changes in atmospheric circulation, I: changes in the mass of large ice sheets, G: changes in the mass of glaciers, T: changes in the terrestrial hydrosphere, P: post-glacial rebound (assuming a time-independent velocity), V_0: tectonic vertical land motion (assuming a time-independent velocity) δV: nonlinear vertical land motion. (Plag, 2006, see there for a detailed discussion of these factors).

The factors that contribute to secular trends with a fingerprint exhibiting large spatial variations on regional to global scales are the post-glacial rebound signal, the steric signal and the present-day contribution from the two large ice sheets in Antarctica and Greenland (Plag, 2006). Moreover, changes in atmospheric circulation are also likely to have regional scales. The database for these factors are discussed in the next Section.

3 The database and methodology

Time series of monthly mean values for LSL are taken from the PSMSL data base (Woodworth & Player, 2003), which contains records from more than 1950 tide gauges, i.e. a major fraction of the global tide gauge data. Those records, for which the history of a local reference can be established are compiled into a subset denoted as *Revised Local Reference* (RLR) datasets, and these records can be used confidently to determine local LSL trends.

Most of the PSMSL records are restricted to the time window of approximately 1950 to 2000. Thus, only in that time interval a spatially sufficient picture of the pattern of LSL trends can be expected. Considering that the steric sea level changes are given for the time window 1950 to 1998 (see below) we choose this time window as a compromise between highest accuracy for the local secular LSL trends and the optimal spatial coverage. For each tide gauge, Plag (2006) determined a secular trend by fitting the model function

$$g(t) = a + bt + \sum_{i=1}^{2} A_i \sin(\omega_i t + \phi_i) \tag{2}$$

to the series of monthly mean sea levels, where t is time, a is an offset and b the constant secular LSL trend. A_i and ϕ_i are the amplitude and phase, respectively, of an annual and semiannual constituent. In the fit, the parameters a and b and the amplitudes of the sine and cosine terms of the annual and semi-annual constituents are determined simultaneously.

Here we use an alternative equation to determine the LSL trends, i.e.

$$g(t) = a + bt + \sum_{i=1}^{2} A_i \sin(\omega_i t + \phi_i) + \sum_{i=1}^{3} d_i \sigma_i \tag{3}$$

where $\sigma_i,\ i = 1,2,3$, are the relevant components of the atmospheric stress tensor on the sea surface, and d_i are the respective regression coefficients, which we determine together with the other parameters in the least squares fit to the LSL records. The component of the atmospheric stress tensor perpendicular to the sea surface is the air pressure p. The horizontal components are taken to be proportional to the wind stress components, i.e.

$$\sigma_2 \;\sim\; w_{\mathrm{E}} \sqrt{w_{\mathrm{E}}^2 + w_{\mathrm{N}}^2} \tag{4}$$

$$\sigma_3 \;\sim\; w_{\mathrm{N}} \sqrt{w_{\mathrm{E}}^2 + w_{\mathrm{N}}^2} \tag{5}$$

where w_{E} and w_{N} are the east and north components of the wind vector, respectively. We denote the sets of

LSL trends determined with eq. (2) and eq. (3) as T1 and T2, respectively.

Monthly mean values of the air pressure and the wind stress components are computed from the ERA40 reanalysis data provided by the *European Center for Medium Range Weather Forecast* (ECMWF). The ERA40 dataset has a spatial and temporal resolution of $2.5° \times 2.5°$ and 6 hours, respectively. Monthly means of σ_2 and σ_3 are computed as averages of the six-hourly values of these quantities.

With respect to thermosteric sea level changes, post-glacial rebound signal and the fingerprints of the two large ice sheets in Antarctica and Greenland, we use the same data base as Plag (2006). Thermosteric sea level variations are computed from observations of the subsurface temperature field. Currently, two global datasets are available, namely Levitus et al. (2000) and Ishii et al. (2003). The two datasets are, to a large extent, based on the same observations; however, different analysis schemes are used to create the gridded datasets. As pointed out by Plag (2006), the sea level trends derived from these two datasets display considerable differences, with the former having more short wavelength variations and a larger range of local trends. The computed sea level changes depend on the depth interval used for the integration. For the Levitus et al. (2000) dataset, steric sea levels are available for 500 m and 3000 m (denoted as L500 and L3000). For the Ishii et al. (2003) dataset, sea levels are only available for 500 m (denoted here as I500). All grids have a spatial resolution of 1°.

For the L500 and L3000 datasets, which are given as annual means, local trends were determined by a least squares fit of a polynomial of degree 1 to the data for each grid point. I500 is given as monthly means, and the model function (2) was used instead. In large parts of the ocean, the thermocline depth is much deeper in the ocean than 500 m. Therefore, L500 and I500 are likely to underestimate the thermosteric sea level variations in these areas.

The large uncertainties in the mass changes of the two large ice sheets in Antarctica and Greenland over the last five decades do not allow to use a spatial fingerprint deduced from observations to represent the contribution of these two ice sheets to LSL. Therefore, based on the static elastic sea level equation (Farrell & Clark, 1976), Plag & Jüttner (2001) determined for each ice sheet a fingerprint function for a constant, unit trend over the complete area of the ice sheet. The resulting Antarctic fingerprint has a distinct zonal component, while the Greenland fingerprint shows more variations with longitude, particularly in the northern hemisphere (Plag, 2006).

The present-day LSL fingerprint of the post-glacial rebound signal (PGS) is fairly well predicted by geophysical models. Plag (2006) used a suite of models (Milne et al., 1999) to study the effect of the uncertainties of the predicted PGS fingerprint in LSL on the global results. Here we also use the same set of models but will not discuss in detail the sensitivity of the global results to the PGS model.

The thermosteric contribution is only given on a 1° by 1° grid. Using a regression based on individual LSL trends at tide gauges would require interpolation and in most cases extrapolation of the steric signal from nearby grid points to the exact tide gauge location. Based on a detailed sensitivity study, Plag (2006) chose to create a gridded dataset of LSL trends instead, assigning a weighted average of all available LSL trends to each grid cell with tide gauges. The sensitivity study also indicated that a grid resolution of $2° \times 2°$ was a reasonable compromise between the accuracy of the individual LSL trends assigned to the grids and the spatial resolution required to capture the main features of the spatial fingerprint of e.g. the post-glacial signal. This 2° grid as defined by the available tide gauges only covers about 3.1% of the global ocean surface. Similar 2° grids were created for all available forcing factors by averaging the 1° grids.

4 Effect of the local atmospheric forcing on LSL

At many stations, a large amount (up to 90%) of the variability of monthly LSL is explained by the regression model according to eq. (3), with a large fraction of the model coming from air pressure and to a lesser extent the two wind stress components. In many areas, the regression coefficient for air pressure is close to the equilibrium value of ~ -10 mm/HPa (Fig. 1). However, close to the equator, where air pressure variations are small, much larger values than that are found.

The relative importance of the local atmospheric forcing depends mainly on the latitude and the coastal geometry. At stations at latitudes outside the $\pm 25°$ band the combined local atmospheric forcing explains most of the intraseasonal variations, while significant interannual to decadal variations are more pronounced in the residuals than in the observations (e.g. Halifax, Cuxhaven, San Francisco, and Sydney). At most stations the main atmospheric contribution is due to air pressure, but at Cuxhaven in the German Bight, the east component of the windstress is by far the dominating contribution.

For the stations on the west coasts of the Americas, the El Niños events are visible in sea level. At

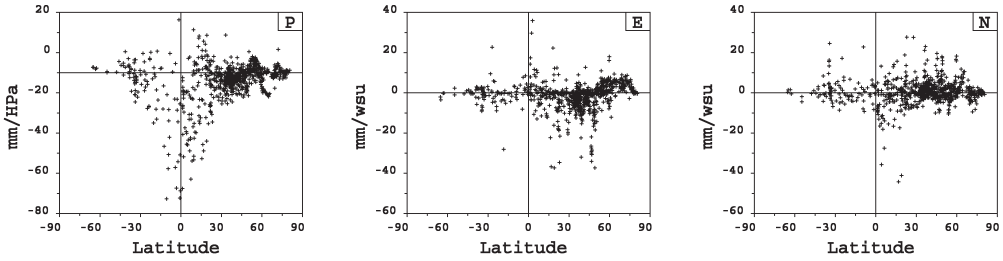

Fig. 1: Regression coefficients for the local atmospheric forcing. P: air pressure, E: east component of wind stress, N: north component of wind stress. The horizontal line in the left diagram indicates the equilibrium value of ≈ -10 mm/HPa.

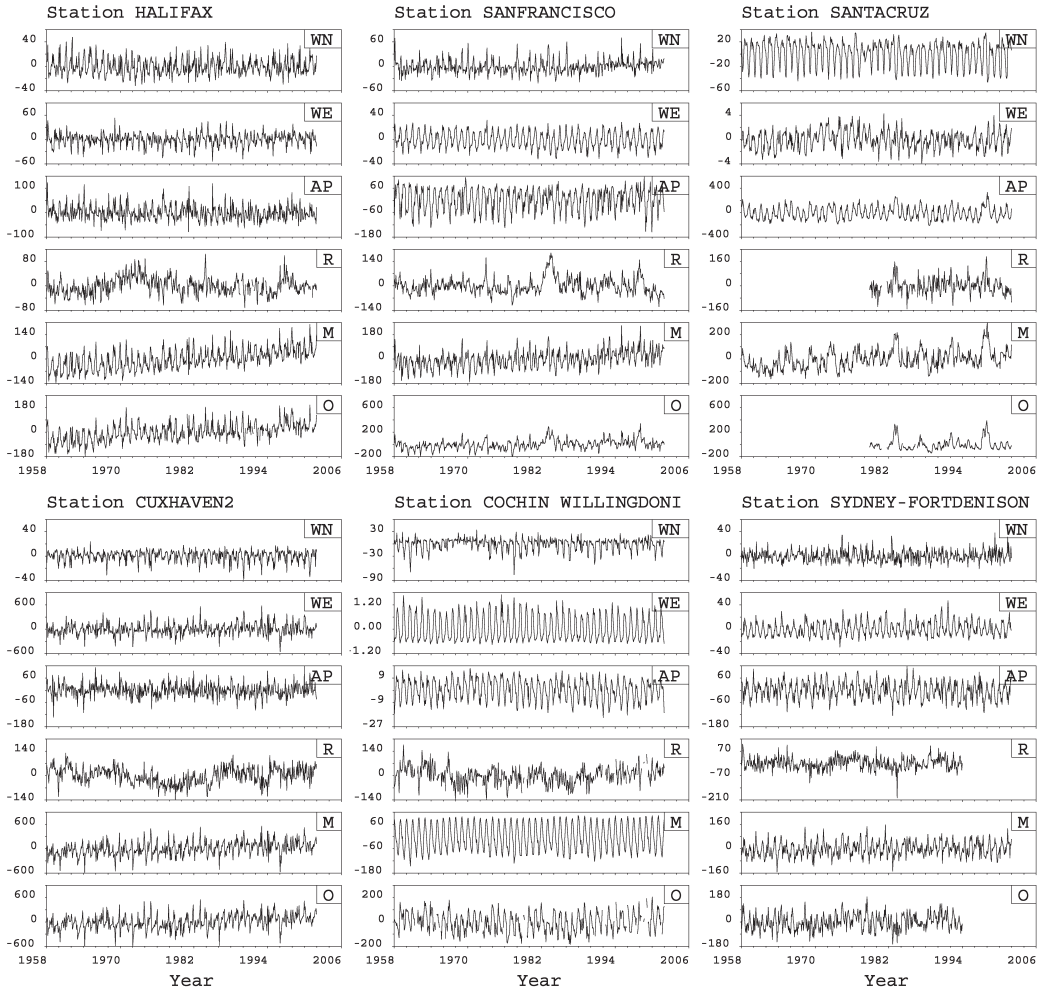

Fig. 2: Regression model for selected tide gauges. For each station, we show O: observations, M: regression model, R: residual, as well as the individual contributions of AP: air pressure, WE: east component of windstress and WN: north component of windstress. All parameters are given in mm.

San Francisco, the high sea levels during the largest El Niños are not modeled by the local atmospheric forcing, while at Santa Cruz in the Galapagos Islands, the local forcing captures a large fraction of these high sea levels very well. However, at Santa Cruz, the regression coefficient for air pressure is as large as -72 mm/HPa, which indicates that there air pressure may be correlated with other factors influencing sea level. At many stations close to the equator, the rather small air pressure variations are dominated by a (likewise) small seasonal signal, which is also present in sea level (e.g. Cochin at the southwest coast of India).

Comparing the LSL grid derived from T1 to the grid derived here from the T2 LSL trends, we see

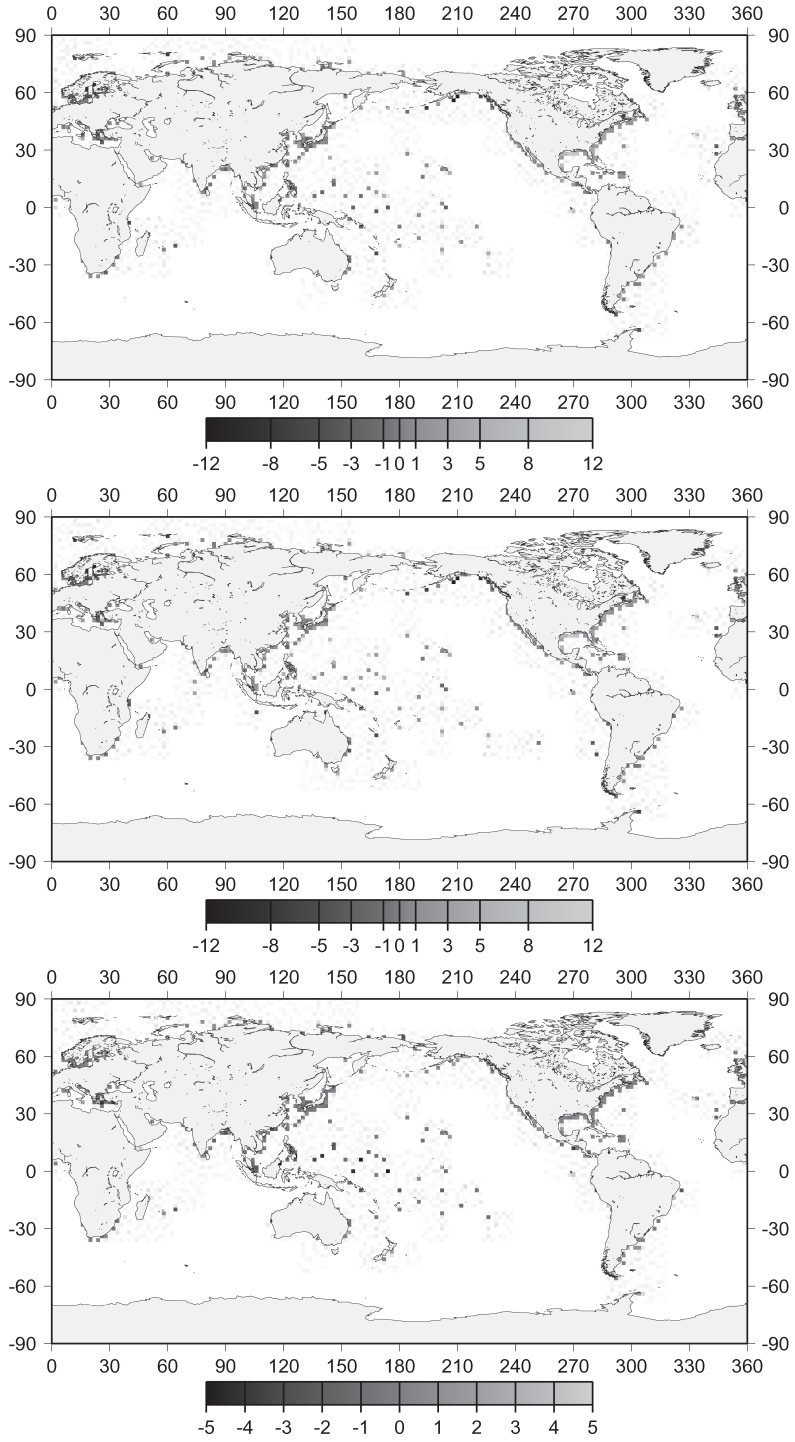

Fig. 3: Effect of local atmospheric forcing on the secular LSL trend pattern. Upper diagram: LSL trend grid derived by Plag (2006) for T1. Middle: LSL trend grid determined in the present study for T2. Lower Diagram: atmospheric contribution to LSL trends computed as the difference between T2 and T1. All scales are in mm/yr. In the computation of the grid values, only local LSL trends within ±12 mm/yr are used and the LSL trends in a grid cell are averaged using the length of the records as weights. Minimum record length is 10 years.

that the spatial pattern shows some differences particularly in the Pacific (Fig. 3). The effect of the atmospheric forcing on the long-term LSL trends depends on the geographical region. For example, along the west coast of North America, the atmospheric contribution in general is positive, exceeding 2 mm/yr in some areas. For most of the North Atlantic, the contribution is also positive, while over the western Pacific, large negative contributions are found reaching -5 mm/yr in some areas. For the Mediterranean stations, the atmospheric contribution is negative (particularly in the Adriatic and the eastern Mediterranean, where it reaches values up to -0.8 mm/yr). The results for the Mediterranean are confirmed by Tsimplis et al.

(2006) on the basis of a hydrodynamical model run.

5 The regression model

The regression model set up by Plag (2006) for the gridded LSL trends is given by

$$\tilde{b}_i = \sum_{j=1}^{K} \alpha_j I_i^{(j)} + \beta P_i + \gamma S_i + c, \qquad (6)$$

where i is the index of the grid cell, $\tilde{b}_i$ is the modeled LSL trend, $I_i^{(j)}$ the LSL trend due to a unit mass change in ice sheet $I^{(j)}$, K the number of individual ice sheet fingerprints included in the regression, P_i the predicted PGS, S_i the thermosteric LSL trend, and c a mean global LSL trend introduced to collect all unaccounted contributions.

The α_j are unknown mean mass trends of the ice sheets, which are determined as a results of the regression analysis. β is introduced to account for any scale error in the PGS predictions. With the introduction of β, we preserve the predicted PGS fingerprint but we allow for adjustments in the amplitude. The same is true for the thermosteric effect, where we have introduce a scale factor γ.

In the following, we have to distinguish between the *regression grid*, which is defined by the fact that all factors used in a regression are available, and the *global (ocean) grid*, which is defined as far as possible for the complete ocean surface. Since all models are available globally, the regression grids are determined as the set of grid cells where both the steric sea level trends and the observed LSL trends are given. The global grids are defined by the steric grid used. The regression grids cover typically 2% of the ocean surface, while the steric grids reach up to approximately 95%.

Any regression analysis is hampered by the presence of high covariance of the forcing factors. Using T1, the fingerprints of the Antarctic and Greenland ice sheet are significantly anti-correlated (Table 1). Moreover, the Greenland ice sheet fingerprint is weakly correlated with the present-day PGS fingerprint. For the steric fingerprints, the correlation with the T1 LSL trends are of the order of 0.25 for the L500 and I500 datasets, while the correlation is less than 0.2 for the L3000 dataset (Table 1).

Using the T2 trends does not change the cross correlation between LSL and most of the factors (Table 1). However, there is no correlation between the steric sea level heights and the T2 trends. In particular, the cross correlation coefficients for I500 and L500 are 0.00 while for L3000 a non-significant value of 0.04 is found.

Taking into account the local atmospheric forcing completely removes the correlation between the LSL and steric trend patterns. This rather surprising results has a profound effect on the results of the regression analysis. It indicates that the steric signal sensed by the tide gauges is mainly due to changes in the upper ocean layer, which appear to be highly correlated with local atmospheric forcing. Thus, a warming of the upper layer and an increase in sea surface temperature will tend to lower the air pressure above the warming area. Both processes will lead to an increase of sea level, which is then fully absorbed in the separate removal of the contribution due to local atmospheric forcing. Nevertheless, in the next section, we will compare selected results to those obtained by Plag (2006) in order to assess the effect of the local atmospheric forcing on the global estimates.

6 Results

In Table 2, results of the regression analysis for a few selected combinations of fingerprints are given for the T1 and T2 LSL trend grids. The actual values of the regression coefficients for T1 are discussed in detail in Plag (2006). Here it is only mentioned that β is in the range of 0.4 to 1.5, depending on the PGS model, while γ ranges from approximately 0.4 for L3000 to approximately 1.2 for I500, depending slightly on the PGS model used. For T2, β is generally lower, while γ is close to zero for all three steric data sets (see below).

For all regressions, the constant c is of the order of 0.5 mm/yr and 0.75 mm/yr for the T1 and T2 LSL trends, respectively. Thus, the unexplained average trend at the tide gauges is between 50 and 80% of the average sea level rise. Moreover, the assumption that c determined for the (small) tide gauge grid can be extrapolated over the whole ocean is uncertain, since most contributions included in eq. (1) are spatially highly variable.

Compared to the T1 results, the T2 results explain a smaller fraction of the spatial pattern in the LSL trends (Table 3). They show a smaller contribution from the Antarctic ice sheet and a larger one from the Greenland ice sheet. The PGS contribution is slightly lower or unchanged, while no contribution comes from the steric forcing. A larger fraction of the LSL trends remains unexplained.

For the T1 solutions, the steric signal based on I500, L500 and L3000 contributes significantly to the global LSL pattern. For the L500 dataset, the explained fraction of the variance is the highest and the

Table 1: Correlation matrix for the fingerprints of the forcing factors and LSL. Columns are: A, G: fingerprints of the Antarctic, and Greenland ice sheets, respectively, P1: post-glacial rebound model (ice history is ICE-3G, upper and lower mantle visocities are $1 \cdot 10^{21}$ and $2 \cdot 10^{21}$ Pas, respectively, and lithosphere thickness is 120 km, see Milne et al. (1999)), I500, L500, L3000: thermosteric fingerprints, and LSL: LSL trend pattern. Matrix is for cross correlation on the regression grid. Upper and lower matrix are for T1 and T2, respectively. For a detailed discussion, see Plag (2006).

	A	G	P1	I500	L500	L3000	LSL
A	1.000	-0.492	-0.118	-0.026	-0.004	-0.120	-0.097
G	-0.492	1.000	-0.187	0.100	-0.023	-0.001	-0.074
P1	-0.118	-0.187	1.000	0.014	-0.006	0.023	0.317
I500	-0.026	0.100	0.014	1.000	0.826	0.675	0.248
L500	-0.004	-0.023	-0.006	0.826	1.000	0.832	0.247
L3000	-0.120	-0.001	0.023	0.675	0.832	1.000	0.186
LSL	-0.097	-0.074	0.317	0.248	0.247	0.186	1.000
A	1.000	-0.493	-0.136	-0.030	0.008	-0.102	-0.088
G	-0.493	1.000	-0.169	0.106	-0.024	0.001	-0.101
P1	-0.136	-0.169	1.000	0.014	-0.007	0.023	0.273
I500	-0.030	0.106	0.014	1.000	0.820	0.676	0.000
L500	0.008	-0.024	-0.007	0.820	1.000	0.827	-0.002
L3000	-0.102	0.001	0.023	0.676	0.827	1.000	0.036
LSL	-0.088	-0.101	0.273	0.000	-0.002	0.036	1.000

Table 2: Selected results of the regression analysis. The column M (Model) indicates the LSL trend set used and gives the factors included in the regression function (6). Parameters are as in eq. (6). The other columns are as follows: E_{mod}: mean of modeled RSL trends, (weighted by area); V: fraction of the variance in % explained by the regression model. For each solution, the upper and lower lines give the regression results in mm/yr equivalent contribution to the mean over the (small) regression grid and the (near-global) complete steric grids, respectively (see Plag, 2006, for a more detailed discussion of the global model). P2 is similar to P1 (see Table 1), except for a lower mantle viscosity of $4.75 \cdot 10^{21}$ Pas. The contributions are given with 95% confidence limits. Bared quantities are spatial averages over the respective grid.

M	$\alpha_{\mathrm{A}} \cdot \bar{I}_{\mathrm{A}}$	$\alpha_{\mathrm{G}} \cdot \bar{I}_{\mathrm{G}}$	$\beta \cdot \bar{P}$	$\gamma \cdot \bar{S}$	c	E_{mod}	V
T1: A,G,P2,I500,c	0.61 ± 0.37	0.04 ± 0.03	-0.09 ± 0.02	0.08 ± 0.02	0.46 ± 0.40	1.10	13.10
	0.27 ± 0.16	0.09 ± 0.07	-0.04 ± 0.01	0.06 ± 0.02	0.46 ± 0.40	0.83	
T2: A,G,P2,I500,c	0.42 ± 0.31	0.07 ± 0.03	-0.07 ± 0.02	0.00 ± 0.02	0.73 ± 0.35	1.15	9.08
	0.19 ± 0.14	0.14 ± 0.06	-0.04 ± 0.01	0.00 ± 0.02	0.73 ± 0.35	1.02	
T1: A,G,P2,L500,c	0.54 ± 0.37	0.02 ± 0.02	-0.12 ± 0.02	0.20 ± 0.04	0.50 ± 0.40	1.14	13.79
	0.24 ± 0.16	0.05 ± 0.05	-0.05 ± 0.01	0.20 ± 0.04	0.50 ± 0.40	0.94	
T2: A,G,P2,L500,c	0.44 ± 0.32	0.06 ± 0.03	-0.09 ± 0.02	-0.02 ± 0.04	0.80 ± 0.35	1.19	9.79
	0.20 ± 0.15	0.14 ± 0.07	-0.04 ± 0.01	-0.02 ± 0.04	0.80 ± 0.35	1.07	
T1: A,G,P2,L3000,c	0.41 ± 0.37	0.02 ± 0.02	-0.12 ± 0.02	0.14 ± 0.04	0.65 ± 0.40	1.10	12.43
	0.18 ± 0.16	0.05 ± 0.05	-0.05 ± 0.01	0.14 ± 0.04	0.65 ± 0.40	0.97	
T2: A,G,P2,L3000,c	0.40 ± 0.32	0.06 ± 0.03	-0.09 ± 0.02	0.01 ± 0.04	0.76 ± 0.35	1.15	9.57
	0.18 ± 0.14	0.13 ± 0.07	-0.04 ± 0.01	0.01 ± 0.04	0.76 ± 0.35	1.04	

regression coefficient is close to one. Based on that, Plag (2006) concluded that the L500 is most consistent with the spatial pattern of the T1 LSL trends. However, in the open ocean, the L3000 set may be better, and for L3000 the global average is 0.35 mm/yr. Consequently, the estimates given in Table 2 for the steric contribution are likely to be at the lower end. However, for the T2 LSL trends, the regression coefficients for all three data sets are very close to zero, leaving no room for a steric contribution.

Table 3: Comparison of T1 and T2 results. The contributions are to global average.

Factor/parameter	T1	T2
Variance explained (%)	11.3 to 13.8	8.5 to 10.1
Antarctica (mm/yr)	0.39±0.11	0.31±0.13
Greenland (mm/yr)	0.10±0.05	0.16±0.03
Thermosteric (mm/yr)	0.30±0.10	0.00±0.01
Unexplained (mm/yr)	0.35±0.40	0.45±0.35
Global average (mm/yr)	0.90±0.75	1.00±0.70

For all regressions, the global average values are lower than the averages obtained for the regression grid, and they are at the very low end of values generally reported for the global sea level rise over the last 50 to 100 years. The basic assumptions for the extrap-

olation of the models from the regression grid to the global grid are: (1) the regression model is appropriately representing the long spatial wave length in sea level trends, and (2) there are no other open ocean contributions to global sea level rise not sensed by the tide gauges, that would affect the extrapolation of c.

Plag (2006) argued that the results for the steric contributions using the L500 and I500 datasets are likely to be minimum estimates, while the global average of the L3000 dataset indicates that the actual steric contribution may be larger by 0.1 to 0.2 mm/yr. Therefore, he considered a global sea level rise value of 1.05 ± 0.75 mm/yr to be more likely. For the T2 results, it is likely that the steric contribution has been absorbed by the regression of local atmospheric forcing. Therefore, if we add a similar contribution to compensate for a bias of the steric contribution, the global average LSL trend for the T2 grid is of the order of 1.20 ± 0.70 mm/yr.

7 Conclusions

The comparison of the regression results for the T1 and T2 LSL trends reveals a high correlation between spatial patterns of the LSL trends locally attributed to atmospheric forcing and the thermosteric contribution. This correlation may be due to a feedback from sea surface temperature changes to the regional air pressure and wind fields.

The regression results for both LSL trend datasets show that the observed spatial pattern of LSL trends is compatible with melting of both the Greenland and Antarctic ice sheets. In fact, the results assign a high significance to this melting.

Based on the regression results for T1, the steric contribution to the global LSL average trend is at least 0.20 ± 0.04 mm/yr but more likely to be larger. However, a part of that signal may actually be due to a correlated effect of atmospheric forcing on sea level.

The results presented here underline the potential of the fingerprint method to extract useful information from the sea level observations provided by the global network of tide gauges. Potential biases of the regression results and particularly the extrapolation to the global ocean surface are discussed by Plag (2006) and can result from (1) long-term changes in the Greenland and Antarctic ice sheets, (2) errors in the PGS predictions, and (3) unaccounted factors with fingerprints having large spatial variations. Here we have identified an additional error source, which results from the correlation of atmospheric forcing and steric changes. In order to reduce the biases, a more comprehensive regression model needs to be set up, that takes into account the different forcing factors in one common fit.

Acknowledgements

The author would like to thank J. Hunter for a thorough review, J.X.Mitrovica for the provision of the post-glacial rebound models, and Anny Cazenave for the provision of the steric sea levels computed from the Levitus and Ishii datasets. The tide gauge data was taken from the database maintained by the *Permanent Service for Mean Sea Level*. Without the long-lasting work of the PSMSL, this study would not have been possible. Part of this work was supported by a NASA grant in the frame of the Interdisciplinary Science Program.

References

Church, J. A., Gregory, J. M., Huybrechts, P., Kuhn, M., Lambeck, K., Nhuan, M. T., Qin, D., & Woodworth, P. L., 2001. Changes in sea level, in *Climate Change 2001: The Scientific Basis. Contribution of Working Group I to the Third Assessment Report of the Intergovernmental Panel on Climate Change*, edited by J. T. Houghton, Y. Ding, D. J. Griggs, M. Noguer, P. J. van der Linden, X. Dai, K. Maskell, & C. A. Johnson, pp. 639–693, Cambridge University Press, Cambridge.

Farrell, W. E. & Clark, J. A., 1976. On postglacial sea level, *Geophys. J. R. Astron. Soc.*, **46**, 647–667.

Ishii, M., Kimoto, M., & Kachi, M., 2003. Historical ocean subsurface temperature analysis with error estimates, *Monthly Weather Rev.*, **131**, 51–73.

Levitus, S., Stephens, C., Antonov, J., & Boyer, T., 2000. Yearly and year-season upper ocean temperature anomaly field, 1948-1998, Tech. rep., U.S. Gov. Printing Office, Washington, D.C.

Milne, G. A., Mitrovica, J. X., & Davis, J. L., 1999. Near-field hydro-isostasy: the implementation of a revised sea-level equation, *Geophys. J. Int.*, **139**, 464–482.

Plag, H.-P., 2006. Recent relative sea level trends: an attempt to quantify the forcing factors, *Phil. Trans. Roy. Soc. London*, In press.

Plag, H.-P. & Jüttner, H.-U., 2001. Inversion of global tide gauge data for present-day ice load changes, in *Proceed. Second Int. Symp. on Environmental research in the Arctic and Fifth Ny-Ålesund Scientific Seminar*, edited by T. Yamanouchi, no. Special Issue, No. 54 in Memoirs of the National Institute of Polar Research, pp. 301–317.

Tsimplis, M. N., Álvarez-Fanjul, E., Gomis, D., Fenoglio-Marc, L., & Pérez, B., 2006. Mediterranean sea level trends: Separating the meteorological and steric effects, *GRL*, In press.

Woodworth, P. & Player, R., 2003. The Permanent Service for Mean Sea Level: an update to the 21st century, *J. Coastal Research*, **19**, 287–295.